ELSEVIER

Molecular dynamics simulations of silicon-fluorine etching

Adam Darcy,* Alema Galijatovic,* Ronald Barth,* Timothy Kenny,* Kristin D. Krantzman,* and Tracy A. Schoolcraft†

**Department of Chemistry, College of Charleston, Charleston, South Carolina*
†Department of Chemistry, Shippensburg University, Shippensburg, Pennsylvania

Molecular dynamics simulations of the reactions between gaseous fluorine atoms and $(SiF_x)_n$ adsorbates on the Si{100} – (2 × 1) surface are performed using the SW potential and compared to simulations with the WWC reparameterization of the SW potential. Theoretical and experimental work has demonstrated that the reactive fluorosilyl layer during silicon–fluorine etching is composed of tower-like adspecies of SiF, SiF_2, and SiF_3 groups. The objective of the simulations is to determine how the chemical composition, mechanism of formation, and energy distribution of the etched gas-phase products depend on the identity of the reacting adsorbate, the incident kinetic energy, and the parameterization of the potential energy function. Three reactions are simulated: F(g) + SiF_3(a), F(g) + SiF_2–SiF_3(a), and F(g) + SiF_2–SiF_2–SiF_3(a). SiF_4 is the major product and Si_2F_6 and Si_3F_8 are minor products. In Si_2F_6 and Si_3F_8, the silicon–fluorine bond that is formed is stronger than the silicon–silicon bond in the molecule and, therefore, the majority of these products have enough energy to dissociate and will fragment before reaching the detector. An S_N2-like mechanism is the primary mechanism responsible for the formation of SiF_4, Si_2F_6, and Si_3F_8. In addition, at higher energies, the simulations have discovered a previously unknown mechanism for the formation of SiF_4, which involves an insertion between a silicon–silicon bond. The results of the simulations with the two potentials differ quite substantially in their prediction of the reactivity of the adsorbates. The SW potential predicts a 2- to 3-eV lower energy threshold for reaction and a much higher reaction cross-section, especially for the SiF_4 product. These results are explained in terms of the differences in the potential energy functions used to describe the silicon–fluorine interactions. In addition, the results are compared to experimental data on silicon–fluorine etching. © 1996 by Elsevier Science Inc.

Keywords: silicon–fluorine etching, molecular dynamics simulations

Color Plates for this article are on page 278.

Address reprint requests to: Kristin D. Krantzman, Department of Chemistry, College of Charleston, Charleston, South Carolina 29424.
Received 3 December 1996; accepted 3 December 1996.

INTRODUCTION

In silicon–fluorine etching, a reactive fluorine plasma is used to etch away a silicon surface. The technological importance of this process has been the impetus for a tremendous amount of experimental work focused on understanding the mechanisms underlying silicon–fluorine etching.[1–8] As the silicon surface is exposed to the plasma gas, a reactive fluorosilyl layer builds on the surface and Si_xF_y molecules desorb into the gas phase. Interestingly, experiments suggest that reactions *within* the fluorosilyl layer do not make a significant contribution to the observed gas-phase products. Rather, gas-phase products are formed through a direct Eley–Rideal type reaction between incoming fluorine atoms and components of the reactive fluorosilyl layer. Experiments have shown that the reactive layer is composed of SiF, SiF_2, and SiF_3 groups.[2,3] SiF_4 is the major gas-phase product, Si_2F_6 and Si_3F_8 are minor products, and radicals such as SiF_2 and SiF_3 are also observed.[1,4–6] The relative amounts of the gas-phase products depend on both surface conditions and the etching species, with the greatest proportion of Si_2F_6 and Si_3F_8 observed with fluorine atoms than with F_2 or XeF_2.

Theoretical work has focused on the use of *ab initio* calculations and molecular dynamics simulations to study reactions between both F atom and F_2 molecules with the Si{100} – (2 × 1) surface.[9–18] A potential energy function with two-body and three-body terms to model silicon–silicon, fluorine–fluorine, and silicon–fluorine interactions was first developed by Stillinger and Weber (SW).[11,19–21] The three-body terms are necessary to model the tetrahedral bonding of silicon. Experimental data are unavailable for interactions of fluorine with a silicon surface and, therefore, the heteronuclear terms were fit to experimental data on gas-phase SiF_x species. Stillinger and Weber used their potential energy function to perform simulations of the reactions of F_2 molecules with the Si{100} – (2 × 1) surface.[11] Srivastava and Garrison discussed both advantages and limitations of the Stillinger–Weber potential in their review of potential energy surfaces used to model chemical reactions at surfaces.[22]

Journal of Molecular Graphics 14:260–271, 1996

655 Avenue of the Americas, New York, NY 10010

0263-7855/97/$15.00
SSDI S0263-7855(96)00080-X

In the first molecular dynamics simulations to study silicon–fluorine etching, Schoolcraft and Garrison used the SW potential energy function to simulate the initial stages of etching of the Si{100} - (2 × 1) surface by 3.0-eV normal incident fluorine atoms.[13] As a result of the simulations, they were able to propose a structure of the reactive fluorosilyl layer. They observed a reaction layer consisting of SiF, SiF_2, SiF_3 species arranged in tower-like structures on the surface, which Feil et al. also observed in a subsequent study of similar simulations with chlorine.[23] Schoolcraft and Garrison determined that an incoming fluorine atom reacts with the SiF_3 adsorbate to produce gas-phase SiF_4 by an S_N2-like mechanism. They hypothesized a similar mechanism for the formation of Si_2F_6 from an SiF_2–SiF_3 absorbate. Prior to the simulations, *ab initio* calculations by Garrison and Goddard determined that SiF_4 is formed by an S_N2-like mechanism in the gas-phase reaction, $F + F_3Si–SiH_3 \rightarrow SiF_4 + SiH_3$.[24] The activation energy for the gas-phase reaction was calculated to be 1.0 ± 0.2 eV, which should be an upper bound for the reaction on the surface.

Experimental work by Lo et al. used SXPS and PSD spectroscopy to study the structure of the reactive layer for the reaction between XeF_2 and the Si{111} – (7 × 7) surface.[7,8] During steady state etching, SiF and SiF_2 groups are in the lower portion of the fluorosilyl layer and the SiF_3 groups are in the top portion. Consequently, Lo et al. concluded that the tower-like structure predicted by theoretical simulations is a probable structure for the reactive layer.

A limitation of the SW parameterization of the SW potential energy function is that it was fit to experimental gas-phase data on SiF_x species and, thus, was not designed to model interactions of fluorine with a silicon surface. To change the SW potential to better model adsorption reactions of fluorine on the Si{100} – (2 × 1) surface, Weakliem, Wu, and Carter (WWC) reparameterized the SW potential for the silicon–fluorine interactions.[15,16] They compared the SW potential with *ab initio* data for the interaction of a fluorine atom with a silicon cluster to model the reconstructed silicon surface and found the SW potential to be too repulsive for both adsorption of fluorine on the Si{100} – (2 × 1) surface and for lateral interactions between fluorines. For example, for the perpendicular approach of an F atom toward the center of a Si dimer bond, the SW potential predicted a well depth of 0.25 eV compared to the quantum mechanical prediction of 3.0 eV. To correct for this, the heteronuclear potential energy function was refit to 42 *ab initio* points on the energy surface in addition to the experimental gas-phase data on SiF_x. The biggest changes were to the parameters and function to describe the Si–Si–F interactions. Schoolcraft et al.[14] and Carter et al.[17,18] used both the SW potential energy function and the WWC reparameterization to study the reactions of F_2 molecules with the Si{100} – (2 × 1) surface. By comparing the results with experiment, it could not be determined which parameterization was better. However, the simulations with both potentials underestimated the amount of difluorination compared to experimental work.

In our previous work,[25] we described simulations with the WWC reparameterization to study the final stage of silicon–fluorine etching: the reaction between gaseous fluorine atoms and reactive $(SiF_x)_n$ adsorbed species to produce gas-phase products. The objective of the simulations was to determine how the chemical composition, mechanism of formation, and energy distribution of the etched gas-phase products depend on the identity of the reacting adsorbate and the incident kinetic energy. To elucidate the atomistic mechanisms, we developed a *Mathematica* notebook[26] to create animations of the chemical reactions from the numerical data. In this article, we describe improvements in the animations that show bond breaking and bond formation as the reaction proceeds.

The sensitivity of the results to the parameterization of the potential energy function is critical in assessing the conclusions of the simulations. Therefore, in this work, the simulations of silicon–fluorine etching with the original SW potential are performed and compared with the previous simulations with the WWC reparameterization. The two potential energy functions differ only in the parameterization of the heteronuclear terms between silicon and fluorine atoms. Nevertheless, they have a substantial difference in the Si–Si bond energy because the energy depends on the three-body heteronuclear terms in addition to the two-body Si–Si term. For example, in gas-phase Si_2F_6, the SW potential predicts a Si–Si bond energy of 2.0 eV, the experimental value, and the WWC potential predicts a value of 4.5 eV. Consequently, lower energy fluorine atoms are needed to induce etching with the SW potential and the reaction cross-sections are much higher.

Molecular dynamics simulations are run for the following elementary reactions: $F(g) + SiF_3(a)$, $F(g) + SiF_2–SiF_3(a)$, and $F(g) + SiF_2–SiF_2–SiF_3(a)$. These adsorbates are chosen because they are thought to be the precursors to the observed products. Incident fluorine atoms are used with kinetic energies ranging from 2.0 to 7.0 eV. Experimentally, the kinetic energies of fluorine atoms used in silicon etching have been determined to range from thermal, 0.026 eV, to 8.0 eV.[27] The reaction probability at room temperature is estimated to be less than 0.01^1, which suggests that it is the very high-energy fluorine atoms at the tail of the Boltzmann distribution that are responsible for spontaneous etching at room temperature. The reaction cross-section, energy distribution, and effective internal energy of each gas-phase product are determined as functions of both the adsorbate type and incident kinetic energy. In addition, the mechanisms for the formation of the etching products are elucidated. The results of the simulations are compared to those with the WWC parameterization.

As in the case with the WWC parameterization, SiF_4 is the major product and Si_2F_6 and Si_3F_8 are minor products. The reaction cross-section is higher with the SW potential energy function and the energy threshold is lower. These differences can be explained in terms of the potential energy functions used to describe the silicon–fluorine interactions. The mechanisms of formation are the same with both parameterizations. The primary mechanism for the formation of SiF_4 is an S_N2-like mechanism. A secondary, higher energy mechanism is also observed in which the incoming fluorine atom approaches the SiF_3 moiety in a front-side attack and inserts between the Si–Si bond. Si_2F_6 and Si_3F_8 are also formed through S_N2-like mechanisms. Interestingly, the Si_2F_6 and Si_3F_8 products have enough energy to dissociate and will fragment into radicals before reaching the detector. This result is not due to either the incident kinetic energy of the incoming fluorine atom or to a limi-

tation in the potential energy functions. Rather, the Si–F bond that is formed releases more energy into the molecule than that needed to break the much weaker Si–Si bond. Consequently, in the experiment, there must be a way for the molecule to dissipate its excess energy before reaching the detector.

The organization of the article is as follows. Section II describes the molecular dynamics simulations and the analysis of the results. In Section III, the mechanisms for reaction, the reaction cross-section, and the energy distribution of the products are presented. In addition, the change in potential energy as a function of time for several reactions is analyzed and is used to explain the observed differences in the simulations with the two potentials. In Section IV, the meaning and importance of the results are discussed in light of experimental data. Conclusions and a summary of the results of the simulations are in Section V.

DESCRIPTION OF THE CALCULATIONS

Molecular dynamics simulations

In molecular dynamics, the classic trajectory of each atom is calculated by integrating Newton's equations of motion given a set of initial conditions. The reliability of the simulations depends strongly on the potential energy function used to describe the interactions between the atoms. In the present simulations, a microcrystallite consisting of six layers of silicon atoms with eight atoms per layer is used to model the Si{100} – (2 × 1) surface and has been described previously.[25] The top layer of silicon atoms is reconstructed into dimers, and the dangling bonds of the surface silicon atoms are saturated with fluorine atoms. A surface dimer is replaced with a $(SiF_x)_n$ adsorbate. An algorithm[29] based on the generalized Langevin equation (GLE) couples the surface to a heat bath and is used to maintain the temperature of the crystal at 300 K. The fluorine atom is brought in with normal incidence at a randomly chosen aiming point above the surface during a randomly chosen vibrational phase of the crystal. A set of 500 trajectories is run with 2.0-, 3.0-, 5.0-, and 7.0-eV fluorine atoms.

Analysis of the results

Mechanisms Through integrating the classic equations of motion, the trajectory of each atom is determined as a function of time. However, a visual picture is needed in order to use this data to elucidate the mechanisms for the formation of products. Previously, we described a *Mathematica* notebook that was designed to convert the numerical data into a visual animation of the chemical reaction.[26] The animations have been improved by incorporating lines between the atoms that illustrate bond formation and bond breaking. The thickness of the line between each atom is scaled as a function of the two-body bond energy between the atoms. When the two-body bond energy is equal to its maximum value, the line is of maximum thickness. As the two-body bond energy decreases to zero, the line becomes narrower until the bond energy is zero and there is no line between the atoms. For the sake of clarity, only lines for the interactions between adsorbate atoms and between adsorbate atoms with the substrate silicon atom directly bonded to the adsorbate are shown.

Reaction cross-section The reaction probability is determined as the fraction of trajectories that etch. However, the reaction probability cannot be directly compared among different types of adsorbates because each adsorbate has a different surface area. The reaction cross-section, in units of angstroms squared (Å^2), is the product of the reaction probability with the surface area available to the incoming fluorine atom. The reaction cross-section measures the actual area of the adsorbate that is reactive and can be compared among different types of adsorbates. To obtain a better statistical distribution, the surface area available to the incoming fluorine atom is limited to the area directly containing and around the adsorbate. An area of 14.3 Å^2 was used with SiF_3, 39.3 Å^2 with SiF_2–SiF_3, and 40.8 Å^2 with SiF_2–SiF_2–SiF_3. Further discussion of the calculation of the reaction cross-section has been described previously.[25]

Analysis of the products A fluorine atom is determined to have etched the surface when it is 10 Å above the surface and has a potential energy less than −5.0 eV, which indicates it is bonded to a silicon atom. The etched product is analyzed by collecting the coordinates of all atoms above the surface. The potential energy of these atoms is calculated and is used to identify the product and the coordinates of the product are performed as an additional check, in which each coordinate is rendered as a sphere and the product is identified visually.

The analysis of the energy distribution of the product is begun when the molecule has a constant center of mass translational energy which is ~12 Å above the surface. The internal energy of the product is obtained by subtracting the center of mass translational energy from the total kinetic energy of the molecule: $E_{int} = E_{kin} - E_{cm}$. The effective internal energy, E_{eff}, is a measure of the stability of the gas-phase product. If E_{eff} is greater than zero, the molecule has enough energy to dissociate and the product will fragment. It is calculated as: $E_{eff} = E_{int} + E_{pot} - E_{eq} - E_{diss}$.[29] E_{pot} and E_{int} are the potential energy and internal kinetic energy of the product, E_{eq} is the potential energy of the product in its equilibrium configuration, and E_{diss} is the energy needed to break the weakest bond in the molecule. E_{eq} is determined by slowly reducing the temperature of the molecule to 0 K, using an algorithm based on the GLE equation[28] and then calculating the potential energy with the resulting coordinates. The dissociation energy for a bond is determined as the difference between E_{eq} of the molecule and E_{eq} of the fragments after the bond is broken.

RESULTS OF THE SIMULATIONS

Mechanisms for etching

1. F(g) + SiF$_3$(a) There are two possible gas-phase products formed by this reaction: SiF_3 radical and SiF_4. The primary mechanism for the formation of SiF_4 is an S_N2-like mechanism, which is illustrated in Figure 1. In this trajectory, the fluorine radical atom is brought in at normal incidence with 5.0 eV of kinetic energy. The fluorine atom approaches the middle of the SiF_3 adsorbate at an angle near

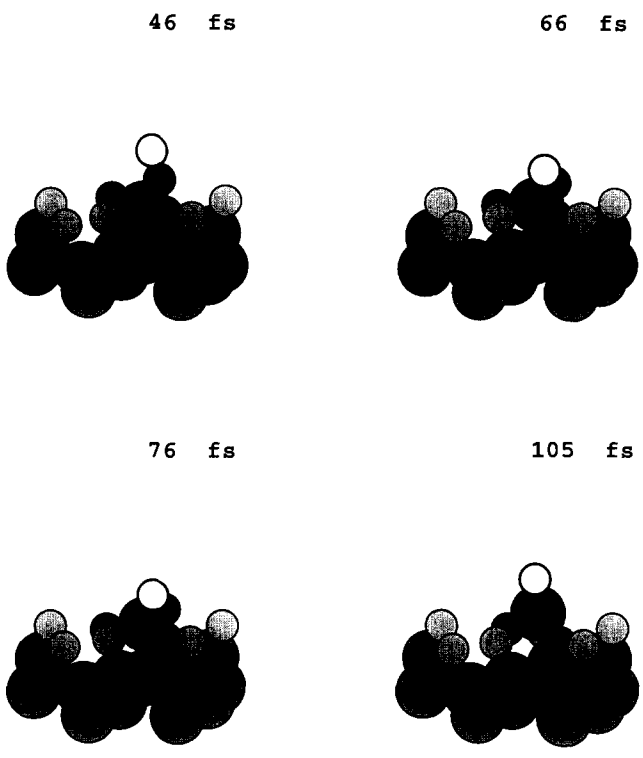

Figure 1. Trajectory for the reaction F(g) + SiF_3(a) → SiF_4(g) by the S_N2-like mechanism. The larger spheres are silicon atoms and the smaller spheres are fluorine atoms. The adsorbate is colored a darker shade of gray. The incoming fluorine atom is a white sphere outlined in black.

180° with respect to the silicon–substrate bond that is broken. At 46 fs, a bond between the incoming fluorine atom and the adsorbate silicon atom begins to form. As the bond is formed, the adsorbate inverts with respect to the plane containing the three fluorine atoms and the silicon–substrate bond begins to break. At 105 fs, the silicon–substrate bond is completely broken and a tetrahedral SiF_4 begins to desorb from the surface.

Figure 2 illustrates the secondary, insertion-like mechanism or the formation of SiF_4, which requires ~2 eV more energy than the S_N2-like mechanism. The fluorine atom approaches the side of the SiF_3 adsorbate and starts to bond to the side of the silicon atom at 56 fs to form a pentacoordinated SiF_4–substrate intermediate complex. The complex sits on the surface for ~190 fs. At 242 fs, the adsorbate slowly rotates on the surface until the incoming fluorine atom can replace the silicon–substrate bond and bond to the silicon atom in a tetrahedral position. Finally, the incoming fluorine atom scoops underneath the adsorbate and pushes SiF_4 off of the surface at 271 fs.

SiF_3 is formed by a replacement-like mechanism illustrated in Figure 3. At 46 fs, the incoming fluorine atom hits an adsorbate fluorine atom and displaces it, forming a bond with the adsorbate silicon atom. At 66 fs, the incoming fluorine bonds has replaced the adsorbate fluorine atom, which rolls down to the surface and adsorbs. SiF_3 radical is formed as the arrangement of fluorine atoms around the silicon becomes trigonal planar and the radical desorbs off of the surface at 193 fs.

2. F(g) + SiF_2–SiF_3(a) Both SiF_4 and Si_2F_6 are major

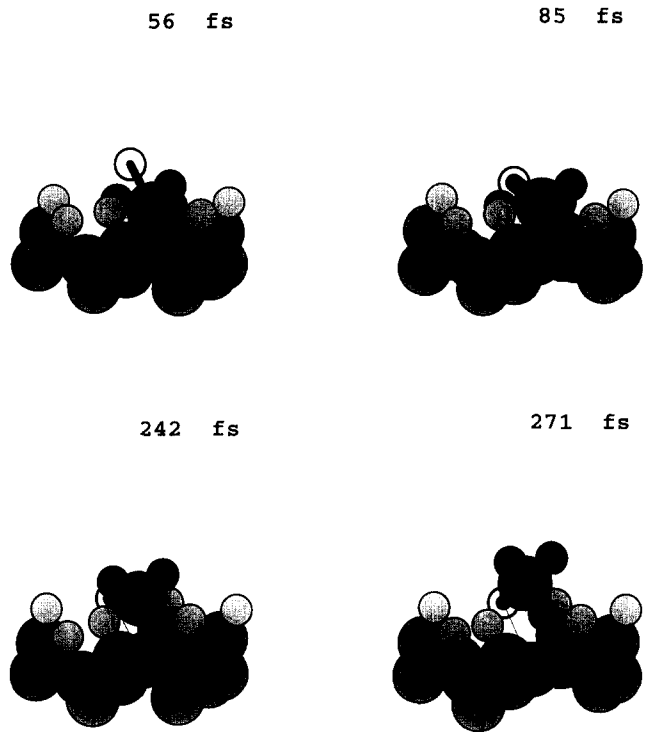

Figure 2. Trajectory for the reaction F(g) + SiF_3(a) → SiF_4(g) by the insertion-like mechanism.

products and the radicals SiF_3 and Si_2F_5 are minor products. As in the case with the SiF_3 adsorbate, SiF_4 is formed by both a S_N2-like mechanism and a secondary insertion-like mechanism. In the S_N2-like mechanism, the fluorine atom

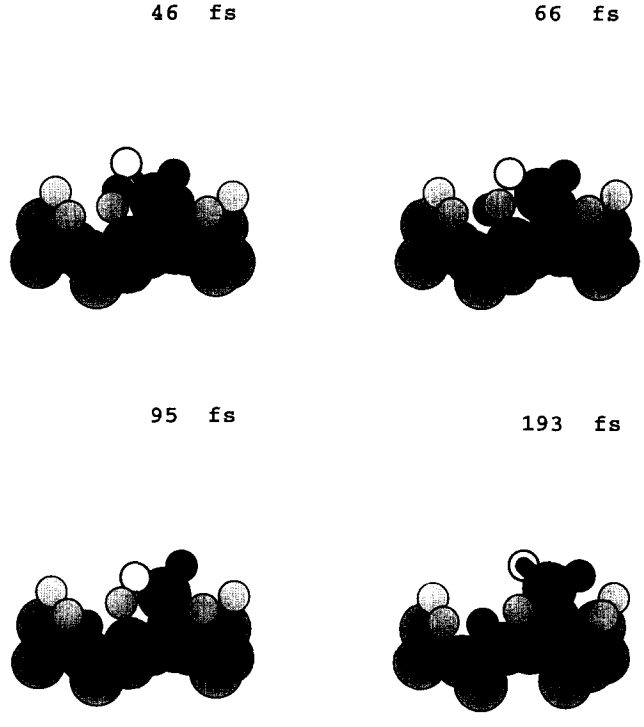

Figure 3. Trajectory for the reaction F(g) + SiF_3(a) → SiF_3(g) by the replacement-like mechanism.

approaches the SiF_3 part of the adsorbate at an angle near 180° with respect to the Si–Si adsorbate bond that is broken. A bond forms between the upper silicon atom and the incoming fluorine atom, SiF_3 inverts, and the Si–Si bond breaks to form gas-phase SiF_4.

In the insertion-like mechanism illustrated in Color Plate 1, on the other hand, the incoming fluorine atom approaches the SiF_3 through a front-side attack between the two adsorbate silicon atoms. Unlike the case with SiF_3, the SiF_2–SiF_3 adsorbate lies almost flat on the surface, and therefore the fluorine atom has almost a perpendicular approach toward the Si–Si bond. As the fluorine atom approaches the SiF_2–SiF_3 adsorbate, it begins to form a bond with both silicon atoms at 46 fs. At 76 fs, the Si–Si adsorbate bond starts to weaken and the upper SiF_3 moiety rotates so that the fluorine atom can bond to it in a tetrahedral position. The fluorine atom inserts between the two silicon atoms, replacing the Si–Si bond and forming SiF_4, which desorbs at 144 fs.

Si_2F_6 is also formed by an S_N2-like mechanism shown in Color Plate 2. However, unlike the case for the formation of SiF_4, the inversion umbrella consists of two fluorine atoms and the upper SiF_3 group rather than three fluorine atoms. The incoming fluorine atom approaches the SiF_2–SiF_3 adsorbate and bonds to the lower silicon atom. As the bond forms between the incoming fluorine atom and the lower silicon atom, the silicon–silicon substrate bond weakens until it is completely broken at 85 fs and the newly formed Si_2F_6 desorbs. In some trajectories, Si_2F_6 dissociates into two SiF_3 fragments as the silicon–fluorine bond is formed.

3. F(g) + SiF_2–SiF_2–SiF_3(a) Three major products are observed with this reaction: SiF_4, Si_2F_6, and Si_3F_8. SiF_4 is formed when F approaches the top silicon atom, Si_2F_6 is formed when F approaches the middle silicon atom, and Si_3F_8 is formed when F approaches the bottom silicon atom. As in the case with the other adsorbates, SiF_4 is formed by both an S_N2-like mechanism and an insertion mechanism. Si_2F_6 and Si_3F_8 are formed by S_N2-like mechanisms.

Figure 4 illustrates the mechanism for formation of Si_2F_6. The upper SiF_3 group of the adsorbate blocks the front side of the SiF_2–SiF_3 group and, therefore, Si_2F_6 can be formed only by a back-side attack. In this case, a very narrow range of aiming points is successful. The incoming fluorine atom must be far enough from the upper SiF_3 group so that it is not repelled. However, it still must be close enough to the adsorbate to feel attraction to the middle silicon atom. As the fluorine atom approaches the middle silicon atom, it draws the silicon atom toward it and a bond begins to form at 76 fs. The silicon–silicon bond starts to break at 105 fs. As the silicon–silicon bond is broken, the silicon–fluorine bond is formed and Si_2F_6 desorbs from the surface at 134 fs.

The mechanism for the formation of Si_3F_8 is shown in Figure 5. The incoming fluorine atom passes by the fluorine atoms of the upper SiF_3 group, bonds to the bottom adsorbate silicon atom, and the silicon–silicon substrate bond breaks. At 154 fs, the newly formed Si_3F_8 begins to desorb from the surface.

Reaction cross-section

1. F(g) + SiF_3(a) The reaction cross-sections with both the SW and WWC potentials as a function of incident kinetic energy are presented in Table 1. The threshold for reaction is ~2 eV with the SW potential and ~5 eV with the WWC potential. This difference can be partially explained in terms of the differences in the Si–Si bond energies. To make SiF_4, a Si–Si bond must be broken, and this bond is

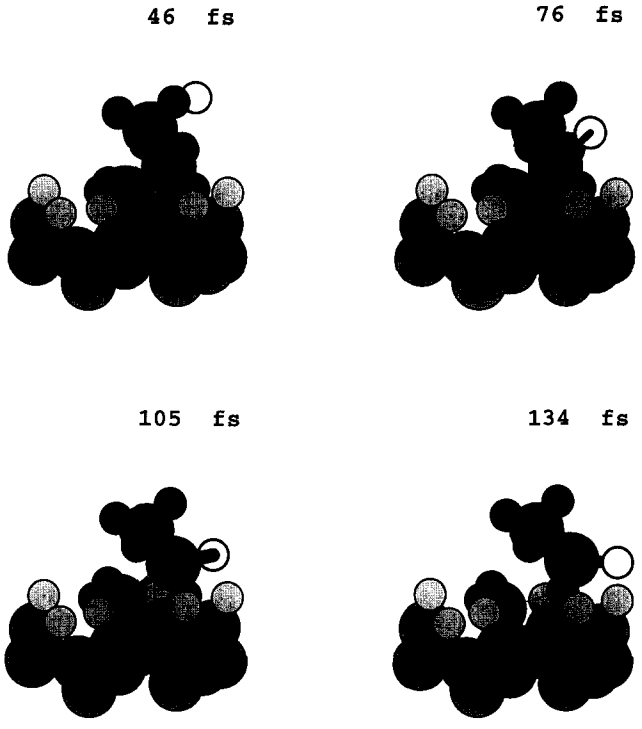

Figure 4. Trajectory for the reaction F(g) + SiF_2–SiF_2–SiF_3(a) → Si_2F_6(g) by the S_N2-like mechanism.

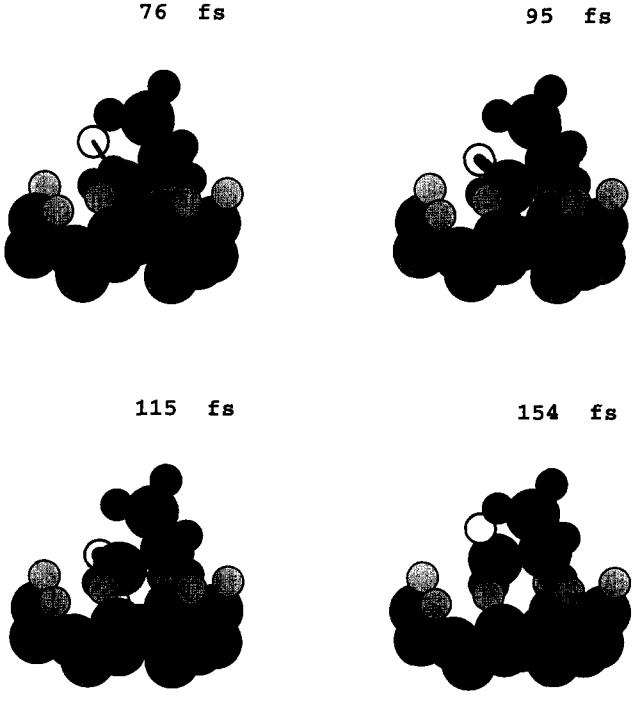

Figure 5. Trajectory for the reaction F(g) + SiF_2–SiF_2–SiF_3(a) → Si_3F_8(g) by the S_N2-like mechanism.

Table 1. Reaction cross-section as a function of kinetic energy

a. F(*g*) + SiF_3(*a*)

Incident kinetic energy (eV)	SiF_4 by S_N2 reaction cross-section (Å^2)		SiF_4 by insertion reaction cross-section (Å^2)		SiF_3 reaction cross-section (Å^2)	
	SW	WWC	SW	WWC	SW	WWC
2.0	0.2	0.0	0.0	0.0	0.0	0.0
3.0	3.4	0.0	0.0	0.0	0.0	0.0
5.0	5.6	0.6	1.0	0.0	0.0	0.0
7.0	5.3	3.3	1.6	0.1	0.3	0.3

b. F(*g*) + SiF_2–SiF_3(*a*)

Incident kinetic energy (eV)	SiF_4 by S_N2 reaction cross-section (Å^2)		SiF_4 insertion reaction cross-section (Å^2)		Si_2F_6 reaction cross-section (Å^2)	
	SW	WWC	SW	WWC	SW	WWC
2.0	0.0	0.0	0.0	0.0	0.9	0.0
3.0	2.5	0.0	0.1	0.0	2.0	1.4
5.0	4.6	0.1	2.6	0.1	3.3	2.7
7.0	5.5	2.0	2.6	0.6	6.1	5.2

c. F(*g*) + SiF_2–SiF_3(*a*)

Incident kinetic energy (eV)	SiF_4 by S_N2 reaction cross-section (Å^2)		SiF_4 by insertion reaction cross-section (Å^2)		Si_2F_6 reaction cross-section (Å^2)		Si_3F_8 reaction cross-section (Å^2)	
	SW	WWC	SW	WWC	SW	WWC	SW	WWC
2.0	1.7	0.0	0.0	0.0	0.0	0.0	0.7	0.0
3.0	4.7	0.0	0.0	0.0	0.0	0.0	0.5	0.0
5.0	5.9	1.8	1.1	0.0	0.7	0.2	1.7	0.4
7.0	5.3	3.1	1.7	0.5	1.2	0.5	2.8	1.1

~2.5 eV weaker with the SW potential. Furthermore, the reaction cross-section is substantially larger with the SW potential. At lower energies, only the fluorine atoms that approach the center of the adsorbate silicon atom are able to react. As the kinetic energy increases, the fluorine atom can overcome the repulsion from the adsorbate fluorine atoms and, consequently, a wider area of aiming points produces SiF_4 by the S_N2-like mechanism and the cross-section increases. The reaction cross-section for the production of SiF_3 is similar with both potentials because the difference between the Si–F bond energies with the two potentials is small.

A comparison of how the potential energy changes as the reaction proceeds provides additional insight into why such substantially different reaction cross-sections are obtained with the two potentials. Figure 6a shows the relative change in the total potential energy as the reaction proceeds for the trajectory in Figure 1. The energy with the SW parameterization, with the WWC parameterization and the difference between the two, $V_{WWC-VSW}$, is plotted as a function of time. In this trajectory for the S_N2 reaction, there is a barrier for the inversion of the SiF_3 group. With the SW parameterization, the barrier is ~2 eV and, with the WWC reparameterization, the barrier is ~5 eV, with a difference of ~3 eV. The biggest changes with the WWC reparameterization are in the Si–Si–F and F–Si–F terms, which depend on the angle at the vertex between the bonds as well as the bond distances. The relative changes in the energy of the Si–Si–F and F–Si–F terms are plotted in Figure 6b and c, respectively. The F–Si–F terms make a larger contribution to the difference in barrier height than the Si–Si–F terms. Therefore, the WWC potential has greater repulsion between the incoming fluorine atom and the adsorbate fluorine atoms, which reduces the reaction cross-section.

Table 1 lists the reaction cross-section for the production of SiF_4 by the insertion mechanism illustrated in Figure 2. The energy threshold is 5.0 eV with the SW potential and 7.0 eV with the WWC potential. Figure 7a illustrates the change in total potential energy with the two different potentials as the reaction proceeds. There is an energy barrier

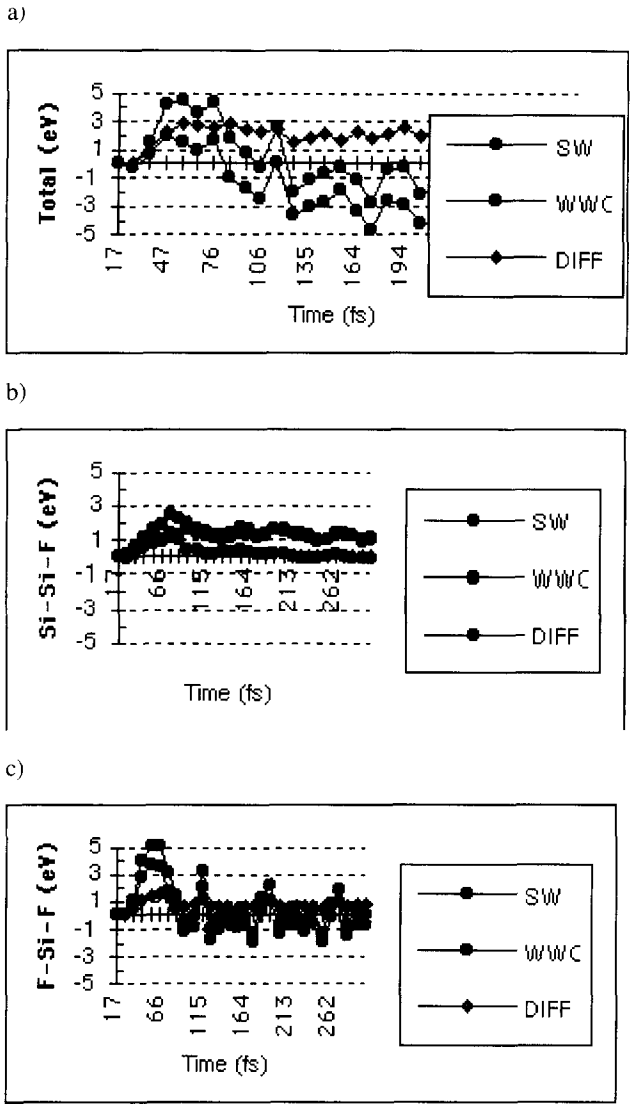

Figure 6. F(g) + SiF_3(a) → SiF_4(g) by the S_N2-like mechanism. (a) Relative change in the total potential energy for the trajectory in Figure 1. (b) Relative change in the Si–Si–F potential energy terms for the trajectory in Figure 1. (c) Relative change in the F–Si–F potential energy terms for the trajectory in Figure 1.

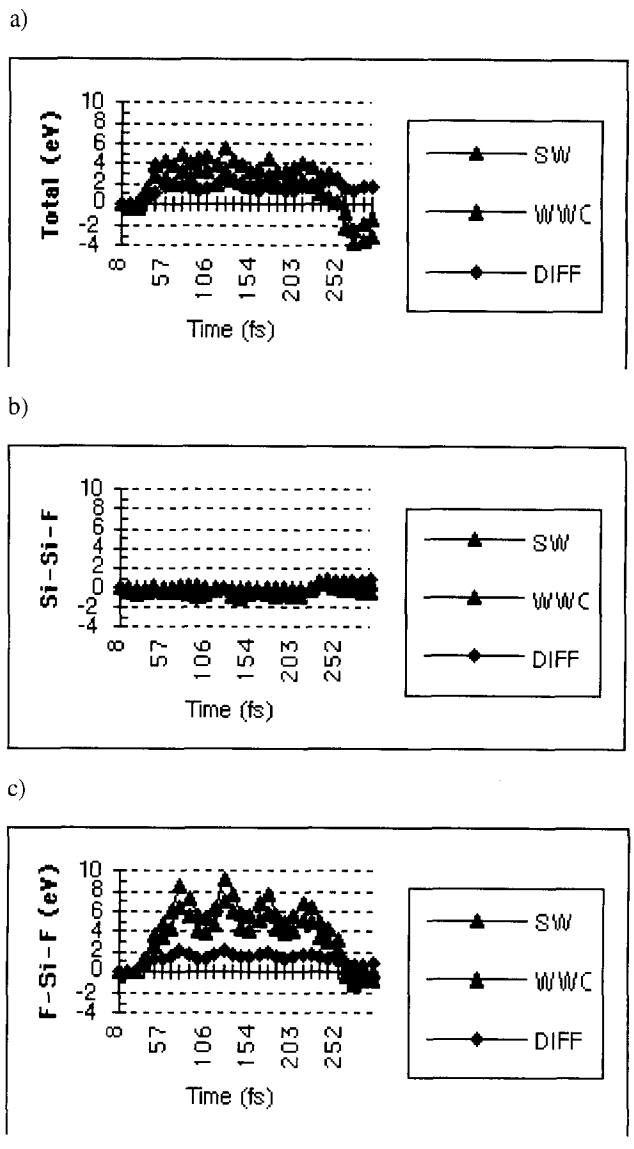

Figure 7. F(g) + SiF_3(a) → SiF_4(g) by the insertion-type mechanism. (a) Relative change in the total potential energy for the trajectory in Figure 2. (b) Relative change in the Si–Si–F potential energy terms for the trajectory in Figure 2. (c) Relative change in the F–Si–F potential energy terms for the trajectory in Figure 2.

for the approach of the fluorine atom to the SiF_3 adsorbate. For this trajectory, the difference in the barrier height between the two potentials is ~2 eV. In this mechanism, the Si–Si–F terms plotted in Figure 7b are more attractive for the incoming fluorine atom with the WWC potential because the fluorine atom is approaching the silicon side of the adsorbate rather than the fluorine side. Recall that the WWC potential was refit to make the adsorption of a fluorine atom onto the Si dimer more attractive. The F–Si–F terms, in Figure 7c, are again more repulsive for the WWC parameterization. The Si–F–F terms are also more repulsive with the WWC potential, thus leading to an overall higher energy barrier.

2. F(g) + SiF_2–SiF_3(a) The reaction cross-sections with both the SW and WWC potentials as a function of incident kinetic energy are in Table 1. As in the case with the SiF_3 adsorbate, the cross-sections for production of SiF_4 by both the S_N2-like and insertion-like mechanisms are much greater with the SW potential. The cross-section for the production of SiF_4 by insertion is highest with this adsorbate because of its placement on the surface. The cross-section for Si_2F_6 has the lowest energy threshold of all the reactions, with a threshold of 2.0 eV with the SW potential and 3.0 eV with the WWC potential. Interestingly, the Si_2F_6 cross-section is similar with the two potentials. Figure 8a shows a plot of the change in total potential energy as a function of time for the trajectory in Color Plate 2. The difference in the barrier height with the two potentials is only ~0.6 eV. Plots of the Si–Si–F terms and F–Si–F terms are in Figure 8b and c, respectively. In this case, the Si–Si–F

a)

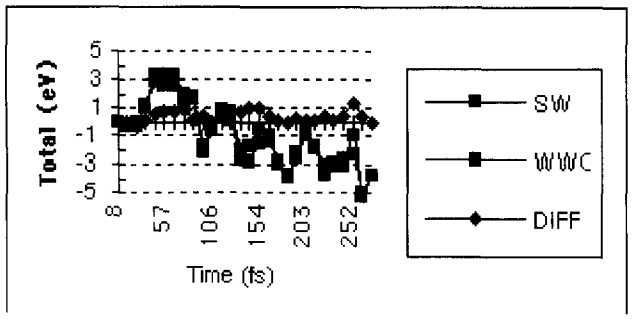

b)

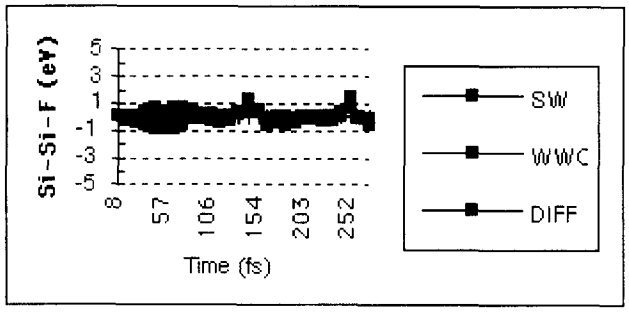

c)

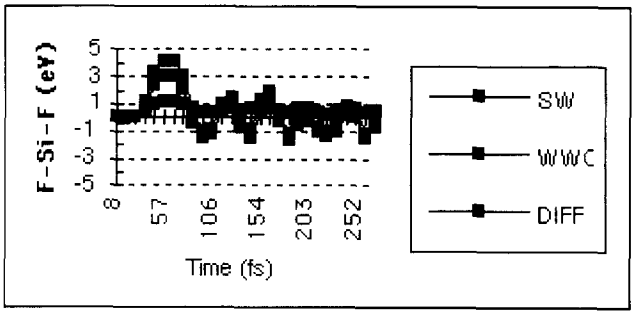

Figure 8. F(g) + SiF_2–SiF_3(a) → Si_2F_6(g) by the S_N2-like mechanism. (a) Relative change in the total potential energy for the trajectory in Color Plate 2. (b) Relative change in the Si–Si–F potential energy terms for the trajectory in Color Plate 2. (c) Relative change in the F–Si–F potential energy terms for the trajectory in Color Plate 2.

terms with the WWC potential are slightly more attractive because of the perpendicular approach to the Si–Si bond. However, unlike the case with SiF_3, the F–Si–F terms are only ~1 eV more repulsive. The F–Si–F terms are less repulsive when approaching SiF_2–SiF_3, because there are only two fluorine atoms undergoing inversion rather than the three fluorine atoms for the formation of SiF_4. Therefore, the Si_2F_6 cross-section is only slightly bigger with the SW potential.

3. F(g) + SiF_2–SiF_2–SiF_3(a) In Table 1, the reaction cross-sections for SiF_4, Si_2F_6, and Si_3F_8 are tabulated as a function of incident kinetic energy for both potentials. SiF_4 is the major product and Si_2F_6 and Si_3F_8 are minor products. Si_2F_6 and Si_3F_8 have smaller reaction cross-sections than SiF_4 because the incoming fluorine atom must overcome repulsion from the upper adsorbate fluorine atoms in order to reach the middle or bottom silicon atom. Si_2F_6 has a particularly small cross-section because of the narrow range of successful aiming points. As in the case with the other two adsorbates, the cross-section for SiF_4 is much larger with the SW potential and the threshold for reaction is ~3 eV lower. The reaction cross-sections for both Si_2F_6 and Si_3F_8 are larger with the SW potential, although the differences are not as great as for SiF_4. In the formation of both of these products, only two fluorine atoms are in the inversion umbrella and, therefore, the difference in the repulsive V_{F-Si-F} terms is less than for SiF_4. The relative change in the total potential energy, the Si–Si–F potential energy terms, and the F–Si–F potential energy terms are plotted as a function of time in Figure 9a–c for the formation of Si_3F_8 illustrated in Figure 5. The difference in barrier height is ~1.5 eV, greater than the ~0.6-eV difference for the formation of Si_2F_6 from SiF_2–SiF_3. The difference is that the Si–Si–F terms are less attractive with the SiF_2–SiF_2–SiF_3 adsorbate because of the angle of approach of the incoming fluorine atom to the Si substrate–Si bond.

Energy distribution

Table 2 lists the center of mass kinetic energy, the average internal energy, the average effective internal energy, and the percentage of the gas-phase product with enough energy to dissociate. The internal energy and the effective internal energy are time averaged over the vibrational fluctuations of the molecule. When the effective internal energy is less than zero, the molecule has enough energy to fragment.

The energy distribution values for the products of the reaction with the SiF_3 adsorbate are listed in Table 2a. At 2.0 eV, SiF_4 is formed by the S_N2 mechanism with the SW potential. SiF_4 leaves with an average of 4.4 eV of kinetic energy, 2.4 eV more than the kinetic energy of the incident fluorine atom. The primary contribution to the kinetic energy of the molecule comes from the energy that is released as the Si–F bond is formed. Consequently, as the incident kinetic energy is increased, the average kinetic energy of the molecule does not increase proportionally. Most of the kinetic energy of the molecule is in the form of internal kinetic energy, which indicates that the molecule has a considerable amount of vibrational and rotational motion. At 2.0 eV, the average effective energy is −1.4 eV, which means that the average molecule has 1.4 eV less energy than that needed to break the 7.0-eV Si–F bond. At 2.0 eV, 0.0% of the molecules have enough energy to dissociate, and at 7.0 eV, 27.4% have enough energy to dissociate. The results with the WWC potential are similar, although the molecules have a lower average effective internal energy because the barrier to reaction is higher. In the insertion-like mechanism, the molecules leave with a lower average effective internal energy because the energy barrier to the reaction is higher. Furthermore, the molecules spend more time on the surface and, therefore, lose more of their energy to the surface.

The results with the SiF_2–SiF_3 adsorbate are listed in Table 2b. The results with SiF_4 are similar to those with the SiF_3 adsorbate. The energy distribution of Si_2F_6 shows an

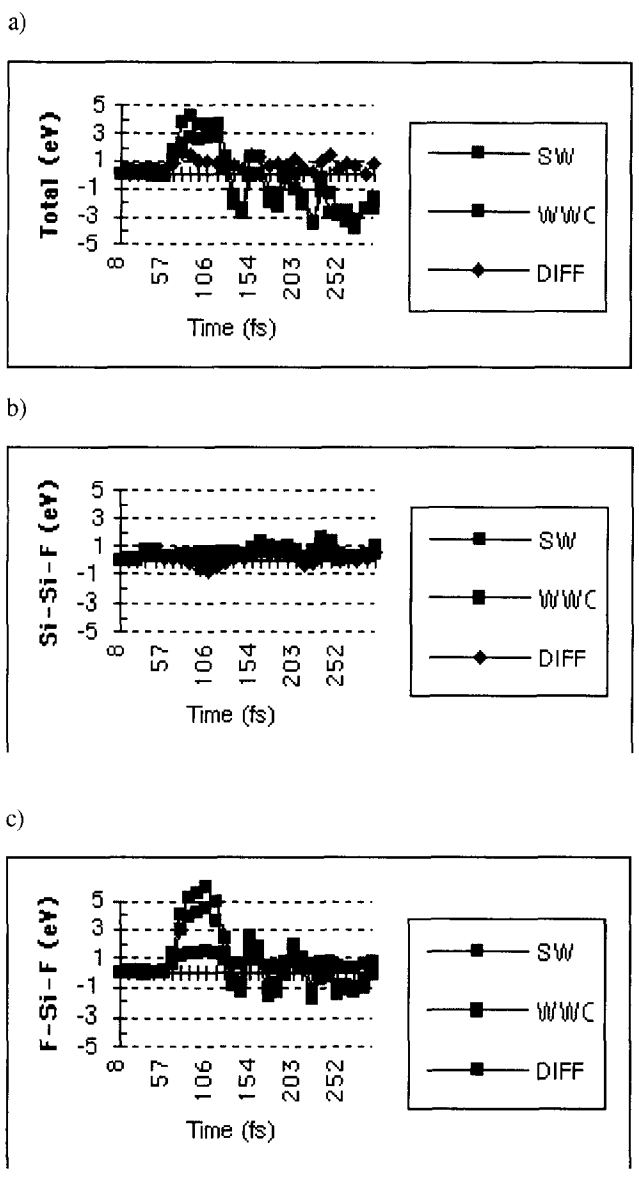

Figure 9. F(g) + SiF_2–SiF_2–SiF_3(a) → Si_3F_8(g) by the S_N2-like mechanism. (a) Relative change in the total potential energy for the trajectory in Figure 6. (b) Relative change in the Si–Si–F potential energy terms for the trajectory in Figure 6. (c) Relative change in the F–Si–F potential energy terms for the trajectory in Figure 6.

interesting result: Nearly all of the molecules have enough energy to dissociate. Si_2F_6 is produced at 2.0 eV with the SW potential. The average molecule leaves with 4.5 eV of energy, which comes from the high exothermicity of the reaction. A total of 7.0 eV is released when the Si–F bond forms, but only 2.0 eV is required to break the Si–Si bond. Consequently, the molecule will have more than enough energy to fragment into SiF_3 radicals. With the WWC potential, 4.4 eV is required to break the Si–Si bond and, therefore, Si_2F_6 will have a lower effective internal energy. Nevertheless, the molecules still have more than enough energy to fragment.

Table 2c shows the results with the SiF_2–SiF_2–SiF_3 adsorbate. Again, the results are similar to those with SiF_2–SiF_3. Most of the SiF_4 is stable at lower incident kinetic energies. None of the Si_2F_6 or Si_3F_8 molecules are stable.

DISCUSSION

Experiments on spontaneous silicon–fluorine etching at room temperature have shown that SiF_4 is the primary product and Si_2F_6 and Si_3F_8 are minor products, with the relative amounts of each product sensitive to surface conditions.[1–8] Note that the actual proportion of each adsorbate on the surface is not known and, therefore, the product distribution cannot be directly compared with experiment. If the ratio of the three adsorbates on the surface is hypothesized to be 1:1:1, then at 5.0 eV the SW potential predicts a product distribution of 78% SiF_4, 15% Si_2F_6, and 6% Si_3F_8 and the WWC potential predicts 46% SiF_4, 49% Si_2F_6, and 8% Si_3F_8. The WWC potential overestimates the importance of the Si_2F_6 product because it was fit to model fluorine adsorption.

The SW potential predicts a lower energy threshold and a higher reaction cross-section for the reactions with all three adsorbates. The WWC potential predicts a threshold energy of 5.0 eV for the production of SiF_4, which seems unlikely from the experimental evidence. Both potentials may overestimate the barrier to reaction compared to the *ab initio* calculations. Consequently, the surface may be reactive at lower incident kinetic energies than predicted by the simulations. The tower-like SiF_2–SiF_2–SiF_3 is most reactive, which suggests that these types of adspecies are important reactants in the etching process.

A puzzling result of the simulations is that both potentials predict that all of the larger mass species, Si_2F_6 and Si_3F_8, will fragment into radicals before reaching the detector. The results at 2.0 eV with the Stillinger–Weber potential clearly show that it is the exothermicity of the reaction that gives these products their excess energy. This is because the silicon–fluorine bond that is formed releases more energy into the product than the relatively smaller energy needed to break the silicon–silicon bond. To become stable, Si_2F_6 and Si_3F_8 must lose the excess energy. Previous theoretical molecular dynamics simulations of etching with ion bombardment determined that the $(SiF_x)_n$ species may be buried deep within pits formed in the surface.[23,30] It is possible that the higher energy Si_2F_6 and Si_3F_8 collide with the walls of the pit as they desorb from the surface, thus releasing the extra energy and becoming stabilized. Simulations have been performed to collide gas-phase products with a wall and show that collisions of the energetic species with a wall remove energy from the gas-phase products and stabilize them. In addition, as molecules are polarizable, it is possible that molecules that desorb at an angle from a planar surface may also lose energy to the surface.

Another finding of the simulations is the determination of the mechanisms responsible for the gas-phase products. The primary mechanism for the formation of SiF_4 is an S_N2-like mechanism in which the incoming fluorine atom abstracts the top SiF_3 group, a mechanism that was determined previously from both molecular dynamics simulations[13] and *ab initio* calculations.[24] The simulations show that an S_N2-like mechanism is responsible for the formation of Si_2F_6 and Si_3F_8 as well. However, the simulations with both potentials

Table 2. Energy distribution of products[a]

a. F(*g*) + SiF_3(*a*)

SiF_4 by S_N2

Incident kinetic energy (eV)	$\langle E_{cm} \rangle$ (eV)		$\langle E_{int} \rangle$ (eV)		$\langle E_{eff} \rangle$ (eV)		Percent dissociated	
	SW	WWC	SW	WWC	SW	WWC	SW	WWC
2.0	1.6	—	2.8	—	−1.4	—		—
3.0	2.0	—	2.6	—	−2.0	—		—
5.0	2.4	1.7	2.7	2.7	−1.6	−1.0	2.6	0.0
7.0	2.5	1.9	3.1	2.9	−0.7	−0.6	27.4	10.5

SiF_4 by insertion

Incident kinetic energy (eV)	$\langle E_{cm} \rangle$ (eV)		$\langle E_{int} \rangle$ (eV)		$\langle E_{eff} \rangle$ (eV)		Percent dissociated	
	SW	WWC	SW	WWC	SW	WWC	SW	WWC
5.0	2.7	—	2.5	—	−2.1	—	3.0	—
7.0	2.8	2.1	3.0	2.5	−1.1	−1.6	16.4	0.0

b. F(*g*) + SiF_2–SiF_3(*a*)

SiF_4 by S_N2

Incident kinetic energy (eV)	$\langle E_{cm} \rangle$ (eV)		$\langle E_{int} \rangle$ (eV)		$\langle E_{eff} \rangle$ (eV)		Percent dissociated	
	SW	WWC	SW	WWC	SW	WWC	SW	WWC
3.0	1.0	—	2.8	—	−1.6	—	0.0	—
5.0	1.4	1.4	3.2	1.8	−1.1	−2.8	13.6	0.0
7.0	1.7	1.4	3.6	3.0	−0.2	−1.0	45.7	11.1

SiF_4 by insertion

Incident kinetic energy (eV)	$\langle E_{cm} \rangle$ (eV)		$\langle E_{int} \rangle$ (eV)		$\langle E_{eff} \rangle$ (eV)		Percent dissociated	
	SW	WWC	SW	WWC	SW	WWC	SW	WWC
3.0	1.6	—	1.8	—	−1.6	—	0.0	—
5.0	1.4	1.4	3.2	1.8	−1.1	−2.8	13.6	0.0
7.0	1.7	1.4	3.6	3.0	−0.2	−1.0	45.7	11.1

Si_2F_6

Incident kinetic energy (eV)	$\langle E_{cm} \rangle$ (eV)		$\langle E_{int} \rangle$ (eV)		$\langle E_{eff} \rangle$ (eV)		Percent dissociated	
	SW	WWC	SW	WWC	SW	WWC	SW	WWC
2.0	1.1	—	2.4	—	3.4	—	100.0	—
3.0	1.2	1.3	2.4	2.9	3.5	1.1	100.0	100.0
5.0	1.6	1.7	2.8	3.1	4.1	1.4	100.0	100.0
7.0	1.9	1.6	2.9	3.5	4.7	2.5	100.0	98.5

$\langle E_{cm} \rangle$ is the average center of mass kinetic energy, $\langle E_{int} \rangle$ is the average internal kinetic energy, $\langle E_{eff} \rangle$ is the average effective internal energy, and percent dissociated is the percentage of products that have enough energy to dissociate

Table 2. *Continued*

c. F(*g*) + SiF_2–SiF_2–SiF_3(*a*)

SiF_4 by S_N2

Incident kinetic energy (eV)	$\langle E_{cm} \rangle$ (eV)		$\langle E_{int} \rangle$ (eV)		$\langle E_{eff} \rangle$ (eV)		Percent dissociated	
	SW	WWC	SW	WWC	SW	WWC	SW	WWC
2.0	0.7	—	2.8	—	−1.7	—	0.0	—
3.0	0.8	—	3.0	—	−1.2	—	4.2	
5.0	1.2	0.9	3.3	2.8	−0.7	−1.2	16.7	0.0
7.0	1.3	1.2	3.8	3.1	0.6	−0.4	69.2	42.1

SiF_4 by insertion

Incident kinetic energy (eV)	$\langle E_{cm} \rangle$ (eV)		$\langle E_{int} \rangle$ (eV)		$\langle E_{eff} \rangle$ (eV)		Percent dissociated	
	SW	WWC	SW	WWC	SW	WWC	SW	WWC
3.0	1.3	—	2.5	—	−2.3	—	0.0	—
5.0	1.4	—	3.3	—	−0.7	—	42.9	—
7.0	1.8	1.7	3.6	2.8	−0.005	−0.8	47.6	16.7

Si_2F_6

Incident kinetic energy (eV)	$\langle E_{cm} \rangle$ (eV)		$\langle E_{int} \rangle$ (eV)		$\langle E_{eff} \rangle$ (eV)		Percent dissociated	
	SW	WWC	SW	WWC	SW	WWC	SW	WWC
5.0	1.4	1.6	2.9	2.9	4.6	1.3	100.0	100.0
7.0	1.8	1.6	3.3	3.1	6.6	1.8	100.0	100.0

Si_3F_8

Incident kinetic energy (eV)	$\langle E_{cm} \rangle$ (eV)		$\langle E_{int} \rangle$ (eV)		$\langle E_{eff} \rangle$ (eV)		Percent dissociated	
	SW	WWC	SW	WWC	SW	WWC	SW	WWC
2.0	0.9	—	2.9	—	4.4	—	100.0	—
3.0	1.2	—	2.8	—	3.7	—	100.0	—
5.0	1.3	1.8	3.1	3.6	4.9	2.6	100.0	100.0
7.0	1.5	2.0	3.7	4.0	8.0	3.6	100.0	100.0

$\langle E_{cm} \rangle$ is the average center of mass kinetic energy, $\langle E_{int} \rangle$ is the average internal kinetic energy, $\langle E_{eff} \rangle$ is the average effective internal energy, and percent dissociated is the percentage of products that have enough energy to dissociate.

show an additional mechanism for the formation of SiF_4 at higher energies. This mechanism involves the formation of a pentacoordinated complex and the insertion of the incoming fluorine atom between a silicon–silicon bond. As the form of the SW potential favors a tetrahedral configuration for silicon, this mechanism may be even more important than predicted by the simulations.

It should be noted that others have proposed that defects created by local heating play an essential role in silicon–fluorine etching.[7,8,15–18] The simulations in these studies use a crystalline substrate. Future studies will involve performing the same molecular dynamics simulations on a defective substrate in order to see the role of defects in promoting etching and in the mechanisms for formation of products.

CONCLUSIONS

Molecular dynamics simulations of the reactions between hyperthermal fluorine atoms and SiF_3, SiF_2–SiF_3, and SiF_2–SiF_2–SiF_3 adsorbates on the Si{100} − (2 × 1) surface have been performed with the SW potential and compared normal to previous results with the WWC potential. Although

the results are different quantitatively with the two potentials, the qualitative results are very similar. We can make three significant conclusions from the results of the simulations.

First, the simulations support the hypothesis that the reactions between incoming fluorine atoms and $(SiF_x)_n$ species are responsible for the observed gas-phase products. If each adsorbate were equally important to etching, the predicted product distribution would be similar to that observed experimentally. The relative amounts of each product depend on the relative amounts of each adsorbate, which are determined by the experimental conditions. The simulations show that the SiF_2–SiF_2–SiF_3 adsorbate is most reactive, which indicates that the tower-like adspecies could play an important role in the etching process.

Second, the simulations predict that Si_2F_6 and Si_3F_8 will fragment before reaching the detector. To be observed experimentally, there must be a mechanism by which they lose their excess energy before reaching the detector. For example, the molecules may become trapped in pits in the reactive layer and lose excess energy as they collide with walls of the pit as they desorb.

Third, the simulations have determined that the primary mechanism for the formation of SiF_4 is an S_N2-like mechanism, which has also been determined by previous simulations. Si_2F_6 and Si_3F_8 are also formed by an S_N2-like mechanism. In addition, the simulations have discovered a secondary mechanism for the production of SiF_4 at higher energies. In this mechanism, a pentacoordinated silicon is formed and the incoming fluorine atom inserts between the Si–Si bond.

ACKNOWLEDGMENTS

Financial support of this work by the Cottrell College Science Award by Research Corporation and the National Science Foundation under a Research Planning Grant No. 9409858 is gratefully acknowledged. In addition, we thank the College of Charleston for financial support by the Department of Chemistry and Biochemistry and by the Research and Development Committee. We also thank Barbara Garrison, Konstantinos Giapis, Francis Houle, Deepak Srivastava, Jory Yarmoff, and Paul Weakliem for interesting and useful discussions of this work.

REFERENCES

1 Winters, H.F. and Coburn, J.W. *Surf. Sci. Rep.* 1992, **14,** 161
2 Stinespring, C.D. and Freedman, A. *Appl. Phys. Lett.* 1986, **48,** 718
3 McFeely, F.R., Morar, J.F., and Himpsel, F.J. *Surf. Sci.* 1986, **165,** 277
4 Winters, H.F. and Plumb, I.C. *J. Vac. Sci. Technol. B* 1991, **9,** 197
5 Winters, H.F. and Haarer, D. *Phys. Rev. B* 1987, **36,** 6613
6 Houle, F.A. *J. Appl. Phys.* 1986, **60,** 3018
7 Lo, C.W., Shuh, D.K., Chakarian, V., Durbin, T.D., Varekamp, P.R., and Yarmoff, J.A. *Phys. Rev. B* 1993, **47,** 15648
8 Lo, C.W., Varekamp, P.R., Shuh, D.K., Durbin, T.D., Chakarian, V., and Yarmoff, J.A. *Surf. Sci.* 1993, **292,** 171
9 Craig, B.I. and Smith P.V. *Surf. Sci.* 1990, **239,** 36
10 Radny, M.W. and Smith, P.V. *Vacuum* 1994, **45,** 292
11 Weber, T.A. and Stillinger, F.H. *J. Chem. Phys.* 1990, **92,** 6239
12 Schoolcraft, T.A. and Garrison, B.J. *J. Vac. Sci. Technol. A.* 1990, **8,** 3496
13 Schoolcraft, T.A. and Garrison, B.J. *J. Am. Chem. Soc.* 1991, **113,** 8221
14. Schoolcraft, T.A., Diehl, A.M., Steel, A.B., and Garrison, B.J. *J. Vac. Sci. Technol. A* 1995, **13,** 1861
15 Weakliem, P.C., Wu, C.J., and Carter, E.A. *Phys. Rev. Lett.* 1992, **69,** 200
16 Weakliem, P.C. and Carter E.A. *J. Chem. Phys.* 1993, **98,** 737
17 Carter, L.E., Khodabandeh, S., Weakliem, P.C., and Carter, E.A. *J. Chem. Phys.* 1994, **100,** 2277
18 Carter, L.E. and Carter, E.A. *J. Vac. Sci. Technol. A* 1994, **12,** 2235
19 Stillinger F.H. and Weber, T.A. *Phys. Rev. B* 1985, **31,** 5262
20 Stillinger, F.H. and Weber, T.A. *J. Chem. Phys.* 1988, **88,** 5123
21 Stillinger, F.H. and Weber, T.A. *Phys. Rev. Lett.* 1989, **62,** 2144
22 Srivastava, D. and Garrison, B.J. *Annu. Rev. Phys. Chem.* 1995, **46,** 373
23 Feil, H., van Zwol, J., de Zwart, S.T., Dieleman, J., and Garrison, B.J. *Phys. Rev. B* 1991, **43,** 13695
24 Garrison, B.J. and Goddard, W.A., III. *Phys. Rev. B* 1987, **36,** 9805
25 Galijatovic, A., Darcy, A., Acree, B., Fullbright, G., McCormac, R., Green, B., and Krantzman, K.D. *J. Phys. Chem.* 1996, **100,** 9471
26 Acree, B., McCormac, R., Weaver, S., and Krantzman, K.D. *J. Chem. Ed.* 1995, **72,** 1077
27 Sommerer, T.J. and Kushner, M.J. *J. Appl. Phys.* 1991, **70,** 1240
28 Berendsen, H.J.C., Postma, J.P., van Gunsteren, W.F., Dinola, A., and Haak, J.R. *J. Chem. Phys.* 1984, **81,** 3684
29 Taylor, R.S. and Garrison, B.J. *Langmuir* 1995, **11,** 1220
30 Barone, M.E. and Graves, D.B. *J. Appl. Phys.* 1995, **77,** 1263